2023 IEEE International Conference on Robotics and Automation (ICRA 2023)
May 29 - June 2, 2023. London, UK

PARSEC: An Aerial Platform for Autonomous Deployment of Self-Anchoring Payloads on Natural Vertical Surfaces

Patrick Spieler*,[1], Skylar X. Wei*,[2], Monica Li[3], Andrew Galassi[4], Kyle Uckert[1], Arash Kalantari[1] and Joel W. Burdick[2]

***Abstract*— PARSEC (Payload Anchoring Robotic System for the Exploration of Cliffs) is an autonomy-equipped aerial manipulator that can deploy self-anchoring payloads on rocky vertical surfaces. It consists of a hexacopter and a two Degrees of Freedom (2 DoF) mass balancing manipulator, which can autonomously deploy a self-anchoring payload from its custom end-effector. The payload anchors itself via an actuated microspine gripper. Payload sensor data is wirelessly transmitted to the primary vehicle during and after deployment. A novel state machine controls the four-stage PARSEC deployment process. First, the rotorcraft brings the payload into contact with the surface and applies a constant 6 N normal force through a feedback control loop to preload the payload microspine gripper. Second, while the rotorcraft maintains the constant normal force, the gripper is commanded to close until engagement with the surface is confirmed through the current feedback sensing. Then, the aerial manipulator pulls with 5 N force on the anchored payload to ensure a secure grip before releasing the package and flying away. We present experimental validation of a successful deployment of a 430 g payload on a vertical vesicular basalt surface.**

I. Introduction

This paper presents an aerial system that can autonomously deploy a self-anchoring sensor payload onto sloped or vertical natural surfaces. Vertical surfaces, steep slopes, and cave walls on Mars are valuable potential future science targets, since they are often associated with geologically interesting features: sites undergoing active modification (e.g., landslides/avalanches, slope streaks), exposed bedrock and/or ice, and as-yet unmodified young features (e.g., fresh crater or actively expanding polar pits). Accessing such geological features via traditional wheeled rovers, such as Curiosity and Perseverance, is difficult, if not impossible. On the contrary, aerial vehicles might access and perform science on these steep regions. Successful demonstration of the first powered flight on Mars by Ingenuity helicopter [1] proved that aerial vehicles can be a viable solution for planetary exploration, and this work has led to future aerial mission concepts that will pursue science objectives on Mars [2] and Titan [3]. However, the flight duration of such rotorcraft is usually very short, which limits the scope of science missions they can perform and makes them less desirable for long duration missions. PARSEC enables a rotorcraft to safely deploy and secure a sensor payload on steep scarps and surfaces, and to perform long duration science studies which are of interest for astrobiology and atmospheric science [4]. Moreover, there are many terrestrial applications for systems that can autonomously deposit sensor nodes on remote or difficult to reach locations. An example Mars mission using PARSEC is illustrated in Fig. 2.

There is an increasing interest in developing aerial manipulators that can reliably and autonomously deliver payloads and interact with steep or complex surfaces. Prior

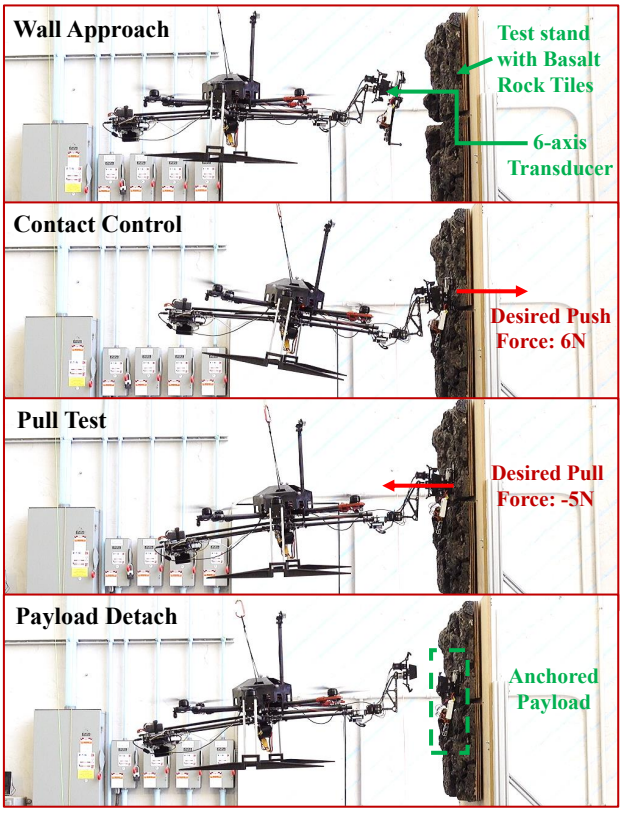

Fig. 1: PARSEC autonomously deploys and anchors a payload on a vertical vesicular basalt wall. Given an anchoring location, a state machine drives the rotorcraft in position flight mode to the vicinity of the target. After the arm is fully extended, PARSEC uses an approach mode until an onboard force sensor detects vertical surface contact. The state machine then switches to a force-based contact mode while a microspine gripper engages. Upon successful engagement confirmation from the payload, the state machine verifies a secure anchor with a pull test. If the pull test is successful, the payload is detached. After arm retraction, the deployment is complete.

* Both author contributed equally.

[1] Patrick Spieler, Kyle Uckert, and Arash Kalantari are with the Jet Propulsion Laboratory, California Institute of Technology, Pasadena, CA, USA. {patrick.spieler, kyle.uckert, arash.kalantari}@jpl.nasa.gov

[2] Skylar X. Wei and Joel W. Burdick are with the Division of Engineering and Applied Sciences, California Institute of Technology, Pasadena, CA, USA. {swei, jburdick}@caltech.edu.

[3] Monica Li is with the Department of Mechanical Engineering at UC Berkeley, Berkeley, CA, USA. monicasli@berkeley.edu.

4 Andrew Galassi is with the Woodruff School of Mechanical Engineering at the Georgia Tech, Atlanta, GA, USA. andrewgalassi@gatech.edu

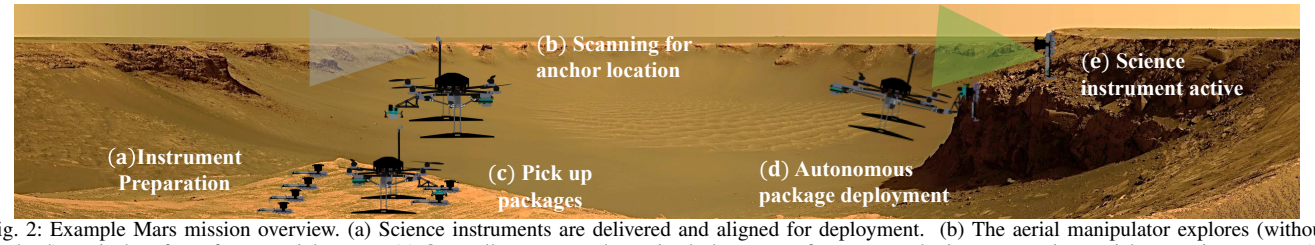

Fig. 2: Example Mars mission overview. (a) Science instruments are delivered and aligned for deployment. (b) The aerial manipulator explores (without payload) vertical surfaces for potential targets. (c) Once all targets are determined, the rotorcraft returns to the instrument site to pick up an instrument. (d) PARSEC first delivers the package to the target vicinity. Via the pre-anchoring approach, gripper engaging, and secure grasp pull test stages, the packages is deployed. (e) Once anchored, the science instruments begin data collection. A similar process retrieves the payloads is a future work.

work includes vehicle perching on vertical surfaces using microspines [5] and gecko-like directional dry adhesive pads [6] or on tree branches [7]–[9] for inspection purposes. Aerial vehicles picking up objects are demonstrated in [10]–[12]. Dual arm aerial manipulators allow collaborative tool inspection and can carry heavy payloads [13], [14]. Deployment and retrieval of sensors are demonstrated in [15].

Aerial manipulators combine agile 6 DoF multirotors with dexterous manipulators. However, commonly underactuated fliers may struggle with manipulator-based physical interactions that require precision, agility, and control of contact forces. For sensor anchoring applications, the movement of the system's center of mass (CoM) due to the manipulation of heavy payloads (e.g., more than 10% of system weight) often requires accurate models, advanced control, and/or compensating mechanical design. In particular, [11] and [12] present designs of counterbalancing arms that use shifting battery weights to minimize CoM movement. Dual arm designs [13], [14] can also achieve self-balancing. There have been several attempts of incorporating force-based contact control with sensor feedback using an underactuated aerial base under quasi-static conditions [16]–[18].

This paper presents PARSEC, a fully autonomous Payload Anchoring Robotic System for the Exploration of Cliffs. The PARSEC platform includes: (1) a custom hexacopter, (2) a novel 2 DoF CoM balancing manipulator arm, (3) a specialized deployment interface at the end of the manipulator, which can carry and deploy (4) a novel and intelligent science payload that self-anchors on vertical surfaces for long-term scientific sampling and monitoring. The custom manipulator design counterbalances the payload mass by shifting the control electronics, minimizing the center of mass shift during manipulator arm and payload movement. The pitch angle of the rotorcraft and the payload are decoupled via a revolute wrist joint. A 6-axis force/torque sensor, integrated at the deployment interface detects contact, helps to regulate pulling and pushing forces, and verifies the security of the payload anchor. A state machine controls the proposed system to ensure a smooth transition across different flight and payload deployment modes, as described in Fig.1, including grasp quality verification to ensure safe package deployment. We experimentally validate this proposed system to verify a secure anchoring and deploy a 430 g payload (significantly heavier than previous studies) on a vertical surface composed of vesicular basalt rock tiles.

This manuscript is organized as follows. We describe the design considerations for this payload deployment task in Section II. Section III details PARSEC's subsystems and mechanical implementation, and Section IV describes the mission architecture and control. Experimental results are found in Section V, and conclusion in Section VI.

II. Task Objective & Design Considerations

The deployment of a self-anchoring science payload offers several novel design and control challenges. Even miniaturized planetary science payloads are comparatively heavy. While visible light cameras are lightweight, miniaturized scientific instruments, such as ultraviolet and near infrared imagers, mini Laser-induced Breakdown Spectroscopy (LIBS), and gas sensors, typically weigh $\sim$500 g. Often, multiple instruments at a single sampling location are needed. Moreover, the payload must contain wireless communication, battery, control electronics, and thermal packaging. Thus, our payloads are heavy compared to previous studies of aerial payload deposition. Considerations of weight distribution throughout the deployment process are crucial.

Moreover, *secure* payload placement requires the rotorcraft to maneuver precisely near the target, and to stably control both pushing and pulling forces over the $\simeq$30 second period during which the self-anchoring micro-spine gripper completes its function. The complex nature of the interaction forces in turn demands sufficient thrust and torque margins. Morever, as the payload transitions from the stowed to deployable configurations, the system must accommodate the CoM shift, including the abrupt change during payload release. Note that the contact forces must be controlled while the heavy payload is at full arm extension. Force/torque sensors are needed to monitor the contact wrenches and verify that the payload is securely anchored to the wall.

A low weight, high thrust rotorcraft is required in order to securely place self-anchoring, heavy science instruments on steep and rugged surfaces. The following sections outline specific subsystem design considerations.

Aerial Base & Manipulator Design: Aerial manipulator designs depend highly on the manipulator mass, payload mass, and the maximum moment and shifts in the CoM. Heuristically, we aim to minimize the ratio of arm to payload mass while: (1) maintaining structure rigidity, (2) maximizing the thrust to power ratio; and (3) minimizing the CoM shift when the arm and payload are displaced. Such a design simplifies the rotorcraft's control system. A practical goal is to optimize the distance between the rotorcraft geometric

center and the propeller tip, since the payload must extend beyond the propellers for safe deployment on a nearly vertical surface. Moreover, a recent Mars Science Helicopter design study [2] found a hexacopter stows tightly in a rocket for transit to Mars and can achieve science objectives.

Our payload anchoring sequence requires the rotorcraft to maintain stable flight in extreme configurations: (1) with and without the payload, at all arm configurations, (2) when the arm end-effector contacts at the anchoring zone and applies both push and pull forces. We concluded that only one DoF is needed to compensate the hexacopter's pitch angle for both gripper preloading and payload angle adjustment to various target slopes. Based on the rotorcraft dimension, the manipulator must extend at least 0.5 meters from the rotorcraft's geometric center, resulting in reductions the pitch control margins if not appropriately designed. Compliance is desirable to modulate impacts thought out the anchoring sequence which is incorporated in the deployment interface instead of in the manipulator.

Deployment Interface and Payload Design: The deployment mechanism and payload must be compact enough to stow during flight. The payload deployment should not create undesirable aerodynamic effects from traversing the propellers' downwash. The payload must anchor reliably on vertical or steep surfaces like the steep scarps on Mars, and anchoring must be verified prior to detachment. The detachment design must account for position and orientation uncertainty of the aerial base relative to the target surface.

A passive compliance between the payload's anchoring system and vehicle frame dampens impact forces when the payload first contacts the target and allows the anchoring system to remain in contact as the vehicle pitches, rolls, and yaws. After deployment, the payload experiences a pitchback moment due to gravity while anchored on a vertical surface. This moment can be minimized by increasing the vertical length of the payload or having the center of mass closer to the wall. In addition, the deployable payload must have an independent power supply and communicate wirelessly with the aerial manipulator during the cooperative deployment.

III. Mechanical Design & Integration

Aerial Base: The hexacopter has six symmetrically placed 13×5.5 dual blade propellers, powered by T-motor U3 700KV brush-less motors. These motors produce a steady thrust of up to 18 N at 16 V input, as benchmarked with a Tyto Robotics 1585 Test Stand. The carbon fiber and aluminum hexacopter frame has a 695 mm wheelbase. Without the manipulator and science payload, the hexacopter take-off weight is 3.57 kg (2.8 kg without battery). The propellers can generate a maximum of 7.32 N·m theoretical pitch or yaw moment, yielding at least 30% pitching and yawing margin at maximum arm extension with maximum payload mass.

2 DoF Manipulator: To minimize mass, we proposed a rigid 2 DoF manipulator (Fig. 3) consisting of a prismatic first joint and a revolute wrist joint. To compensate for the movement of the payload from a stowed to a deployable configuration, and loss of mass after payload deployment, we incorporate a mass counterbalancing mechanism. Similar to [11] and [12], we passively compensate the moving CoM by displacing the onboard computer, auxiliary battery, and electronics in the opposite direction as the payload. The prismatic joint is a novel (over-constrained) 6-bar mechanism powered by two lightweight linear actuators. By retracting the linear actuators, the payload and the $\simeq$ 0.7 kg counterbalancing mass is synchronously extends, enforcing a nearly negligible CoM shift. For a 430 g payload, at full manipulator extension or retraction, with and without the payload, the system CoM shift lies within ± 6 cm, enabling us to treat the moment due to CoM shift as disturbances. For a 500 g science instrument (resulting in a 1 kg payload), the main battery can be grouped with the other counterbalancing electronic components. Despite a discrete CoM change occurs when the payload is disengaged, the resulting pitch back moment assists the vehicle to distant from the wall.

To minimize manipulator weight, the links are made out of carbon fiber tubes and sheets. Bearings on all passive revolute joints reduce friction, and minimize actuation forces. The airframe support the track actuators (Actuonix T16) further reduces redundant support structures. A telescoping carbon fiber tubes is incorporated along the extension axis of the linear stage to add extra rigidity. For lighter payloads, removing the telescoping rod can increase the manipulator to 3 DoF. The magnetic encoder of a Dynamixel MX64 servo provides feedback at the revolute wrist joint, which decouples the aerial base and end-effector pitch orientations.

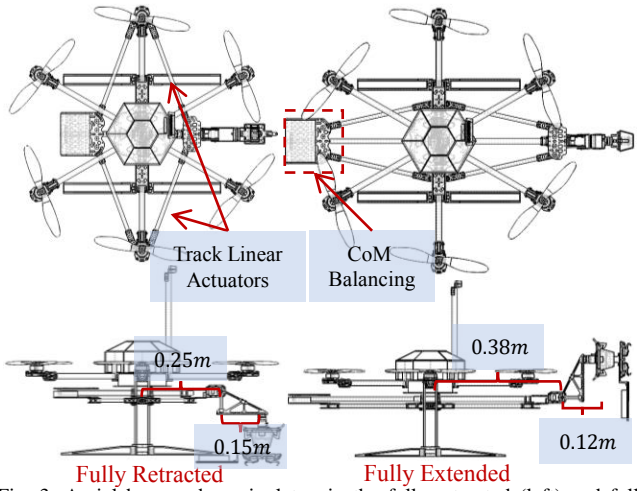

Fig. 3: Aerial base and manipulator, in the fully retracted (left) and fully deployed (right) configurations. The linear stage is driven by the two tracked linear actuators moving synchronously to deploy and retracted the payload. The wrist servo motor compensates the pitching angle of the aerial based.

Deployment Interface: The payload deployment interface is a geometrically interlocking mechanism for smooth payload deployment and reattachment (Fig. 4A). A convex square shell is fixed to the manipulator and the complementary concave shape is fixed to the payload. The convex shell (7 cm sides and 4.5 cm depth) has a 15° taper. The square edges prevent rotational misalignments between the payload and arm. Two cable-driven, rotational clasps on the arm side interface with mating payload features. The clasping features

have a 60° engagement angle and are 2.2 cm from the center of rotation. Once engaged, the interlocking clasps keep the square parts together. A 6 DoF force/torque sensor (ATI Nano 25) rigidly mounts in-line at the deployment interface to detect contact forces and verify anchoring. Closed cell foam in compression between the deployment interface and anchor implements compliance. A center locating pin inhibits translational motion. Hardstops restrict roll to 15° and pitch to 10°. This design encourages anchor contact with slanted surfaces, even if the aerial base pitches and yaws. The interface and payload structure are built from lightweight 3D-printed micro carbon fiber filled nylon.

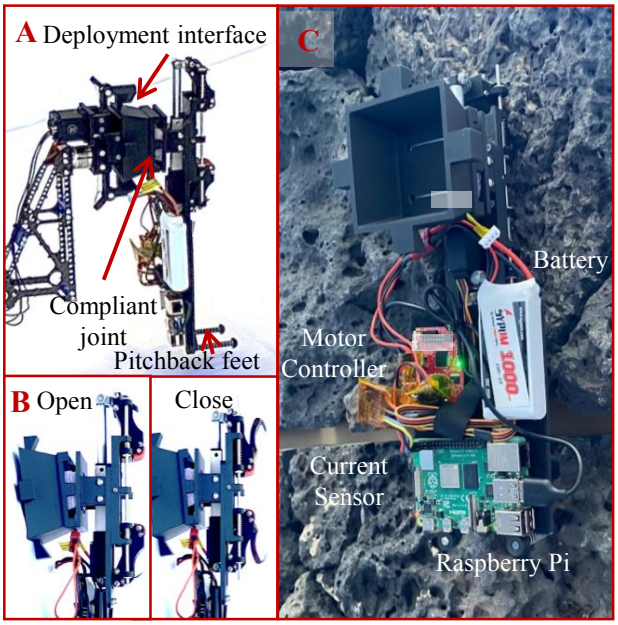

Fig. 4: Payload and deployment interface. (A) Deployment interface linking the manipulator and payload. Payload has passively compliant pitch and roll joints and two pitchback feet. (B) Microspine anchor in open and closed configuration. (C) Payload after anchoring on a basalt wall.

Payload with Microspine Anchor: We use the microspine anchor from [5], an opposed grasper that adheres to a wide variety of rough and textured surfaces (Fig. 4B). This compact and lightweight anchoring mechanism stays anchored for more than 24 hrs with a >1 kg payload. Prior experiments have shown that if the microspine anchor can sustain a 5 N wall-normal pull force, it can support 10 N shear force [5], which exceeds the payload weight. The payload has a $35\text{cm} \times 20\text{cm} \times 15\text{cm}$ bounding volume. In the deployed configuration (Fig. 4C), the anchor and arm interface are seen at the top, with electronics and science payload at the bottom. The spring-loaded pitchback feet are 22 cm below the anchor center and spaced 5.5 cm apart. They enhance payload stability on uneven surfaces.

IV. Mission Architecture and Controls

The conceptual Mars science payload anchoring mission (Fig. 2) includes five phases: instrument preparation, payload pickup, target scanning, autonomous package deployment, and science instrument operations. This section focuses on the autonomy and control methods that enable payload deployment onto a cliff wall. The deployment phase starts off with the rotorcraft flying in the proximity of the vertical cliff and extending the manipulator in preparation for payload anchoring– we assume a suitable deployment location has already been identified. The task is to approach the deployment target in the direction normal to the vertical surface until contact is detected, to maintain contact while the microspine gripper grasps the wall, to perform a pull test which assesses the grasp quality, to release the payload, and to finally detach from the payload, flying away and leaving the payload anchored to the cliff wall. Fig. 1 captures our system performing these steps during one experiment.

It is critical that the control system can transition between flight mode and contact mode without discontinuity in the commanded thrust. In order to achieve this, our mission architecture integrates all flight stages to produce continuous desired attitude and thrust level commands that are tracked by the PX4 autopilot, an open-source software [19].

The rotorcraft is actively controlled in four flight modes: (A) waypoint flight mode, (B) approach mode, (C) contact mode, and (D) detach mode. In the position controlled waypoint flight mode, the system stably tracks a given waypoint and the commanded manipulator joint angles (with or without an attached payload). Once an anchoring waypoint is selected, the arm is fully extended. Then, the system switches into approach mode. As soon as wall contact is detected using the 6-axis load cell, the contact mode is triggered. In this mode, a steady contact force is applied while the microspine gripper grasps the wall. After a grasp completion, a pull test is performed by triggering the detach mode with the payload still connected to the hexacopter. The pull test is successful if the drone does not detach from the wall. In this case, the payload is released, and the the rotorcraft flies away freely. Fig. 6 diagrams the transitions between these modes. The following subsections provide details on the individual modes and their experimental validation.

Waypoint Flight Mode: In waypoint flight mode, the hexacopter controls its position and heading in the inertial frame $\mathcal{I}$. Position setpoints $\boldsymbol{p}_{\mathcal{I}}^{d}$ provide smooth interpolation to the next waypoint. The heading setpoint ψ^{d} is similarly interpolated to the heading of the next desired waypoint. Position is controlled via a Proportional Integral Derivative (PID) controller with saturation on the integral term $\boldsymbol{\xi}$ to $\pm\boldsymbol{\xi}_{max}$ as well as saturation on the position error to limit the flight velocity to $\pm\boldsymbol{v}_{max}$.

$$\boldsymbol{v}_{\mathcal{I}}^{r} = \text{clamp}(\dot{\boldsymbol{p}}_{\mathcal{I}}^{d} - \boldsymbol{K}_{p}(\boldsymbol{p}_{\mathcal{I}} - \boldsymbol{p}_{\mathcal{I}}^{d}), -\boldsymbol{v}_{max}, \boldsymbol{v}_{max}) \quad (1)$$

$$\boldsymbol{t}_{\mathcal{I}} = -\boldsymbol{K}_{d}(\boldsymbol{v}_{\mathcal{I}} - \boldsymbol{v}_{\mathcal{I}}^{r}) - \boldsymbol{\xi} \quad (2)$$

$$\dot{\boldsymbol{\xi}} = \begin{cases} 0 & \text{if } \boldsymbol{\xi} \geq \boldsymbol{\xi}_{max} \text{ and } \boldsymbol{v}_{\mathcal{I}} - \boldsymbol{v}_{\mathcal{I}}^{r} > 0 \\ 0 & \text{if } \boldsymbol{\xi} \leq -\boldsymbol{\xi}_{max} \text{ and } \boldsymbol{v}_{\mathcal{I}} - \boldsymbol{v}_{\mathcal{I}}^{r} < 0 \\ \boldsymbol{K}_{i}(\boldsymbol{v}_{\mathcal{I}} - \boldsymbol{v}_{\mathcal{I}}^{r}), & \text{otherwise} \end{cases} \quad (3)$$

where $\boldsymbol{K}_{p}$, $\boldsymbol{K}_{i}$ and $\boldsymbol{K}_{d}$ are constant positive diagonal gain matrices, while $\boldsymbol{p}_{\mathcal{I}}$ and position and velocity vectors $\boldsymbol{v}_{\mathcal{I}}$ are defined in inertial frame $\mathcal{I}$. The clamp function $\text{clamp}(\boldsymbol{x}, \boldsymbol{x}_{min}, \boldsymbol{x}_{max})$ applies the min, max operations elementwise: $\min(\max(\boldsymbol{x}, \boldsymbol{x}_{min}), \boldsymbol{x}_{max})$.

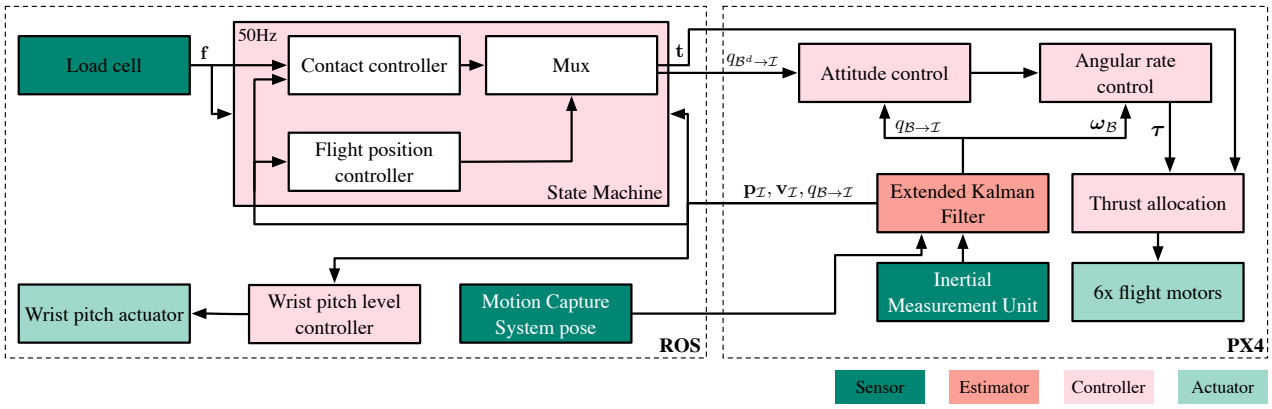

Fig. 5: Control architecture with custom position and contact force controller running on ROS and the PX4 flight controller controlling attitude. $\boldsymbol{\omega}_{\mathcal{B}}$ is the angular rate in body frame and $\boldsymbol{\tau}$ is the moment to be applied.

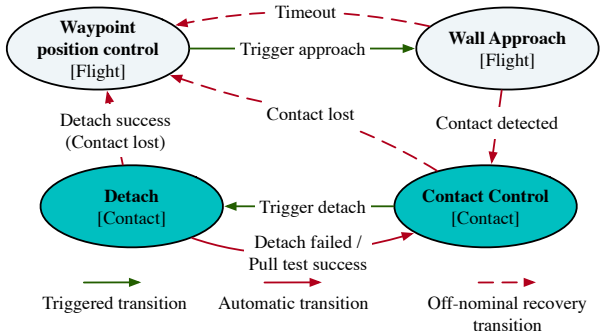

Fig. 6: State machine diagram of the transitions among control modes.

From the computed thrust vector $\boldsymbol{t}_{\mathcal{I}}$ in inertial frame and a yaw setpoint ψ^d the reference attitude quaternion $q_{\mathcal{B}^d\to\mathcal{I}}$ to be tracked by the low level attitude controller is computed:

$$q_{\mathcal{Y}\to\mathcal{I}} = \left[\cos\frac{\psi^d}{2}, 0, 0, \sin\frac{\psi^d}{2}\right] \tag{4}$$

$$\boldsymbol{t}_{\mathcal{Y}} = \boldsymbol{R}(q_{\mathcal{Y}\to\mathcal{I}})^{-1}\boldsymbol{t}_{\mathcal{I}}, \qquad \boldsymbol{t}_{\mathcal{B}^d} = [0,0,1]^\top \tag{5}$$

$$q_{\mathcal{B}^d\to\mathcal{Y}} = \text{shortest\_rotation}(\boldsymbol{t}_{\mathcal{B}^d}, \boldsymbol{t}_{\mathcal{Y}}) \tag{6}$$

$$q_{\mathcal{B}^d\to\mathcal{I}} = q_{\mathcal{Y}\to\mathcal{I}} \circ q_{\mathcal{B}^d\to\mathcal{Y}} \tag{7}$$

where $\boldsymbol{R}(\cdot) \in SO(3)$ is a quaternion equivalent, $\circ$ denotes quaternion product, and $\text{shortest\_rotation}(\boldsymbol{x}_1, \boldsymbol{x}_2)$ is the shortest rotation between $\boldsymbol{x}_1$ and $\boldsymbol{x}_2$ (in quaternion form).

Approach Flight Mode: Approach mode uses the same position controller as waypoint mode. The desired positions $\boldsymbol{p}^d_{\mathcal{I}}$ arise from a constant velocity trajectory towards the wall direction. Approach mode also monitors the load cell to detect wall contact, which triggers the transition to contact mode when nomral forces exceeds 3 N.

Contact Mode: In this mode, the contact force exerted onto the wall is controlled by rotorcraft's attitude and thrust. We define a wall reference frame $\mathcal{W}$ with z-axis aligned with gravity and with x-axis normal to the roughly vertical wall. To optimize the anchoring process, the desired contact force $\boldsymbol{f}^d_{\mathcal{W}}$ is set to a constant 6 N normal force with no side forces. An integral controller on the wall force error generates a desired thrust vector, with $\boldsymbol{K}_c$ a positive diagonal matrix:

$$\dot{\boldsymbol{t}}_{\mathcal{W}} = -\boldsymbol{K}_c(\boldsymbol{f}_{\mathcal{W}} - \boldsymbol{f}^d_{\mathcal{W}}) \tag{8}$$

$$q_{\mathcal{B}^d\to\mathcal{W}} = \text{shortest\_rotation}(\boldsymbol{t}_{\mathcal{B}^d}, \boldsymbol{t}_{\mathcal{W}}) \tag{9}$$

$$q_{\mathcal{B}^d\to\mathcal{I}} = q_{\mathcal{W}\to\mathcal{I}} \circ q_{\mathcal{B}^d\to\mathcal{W}} \tag{10}$$

The wall contact force $\boldsymbol{f}$ is measured by the 6-axis load cell in the end-effector frame. This contact force is transformed to frame $\mathcal{W}$ using the wrist angle and body attitude estimate.

On transition from flight to contact, the initial thrust vector $\boldsymbol{t}_{\mathcal{W}}$ is chosen to avoid a discontinuity in the thrust command. At the transition back to flight mode, the integrator value $\boldsymbol{\xi}$ is similarly initialized from $\boldsymbol{t}_{\mathcal{W}}$ to avoid a thrust discontinuity.

Detach Mode: This mode has two roles: (1) When the payload anchored to the wall is released from the arm, this mode drives the hexacopter away from the wall. (2) While the payload is anchored to the wall, but still fixed to the arm, detach mode validates anchoring quality by a pull test.

Detach mode uses the same contact controller as described above, but the desired normal force ramps linearly from 6 N push to a 5 N pull over a 2 s period. If the package is securely anchored, the state machine switches back to contact mode to apply a pushing force again. If contact is lost, the hexacopter transitions to the waypoint flight mode and holds a position away from the wall. Contact loss is detected in one of two ways: The rotorcraft moves more than 0.5 m from the target, or the measured pull force is less than 20% of the commanded pull force, 2 s after completing the contact force setpoint ramp.

Manipulator Control: The arm's extension / retraction, along with wrist unfolding, is controlled by a mission sequence within waypoint flight mode. The wrist keeps the payload level during the approach, contact & detach modes.

Payload Microspine Gripper Actuation: The payload's microspine gripper closes after stable wall contact is made. Motor current in the gripper closing actuator is used as a proxy for gripper closing force. A constant voltage is applied to the motor until a current threshold is reached, which indicates a solid grasp. The pull test validates grasp quality.

V. Experimental Validation

To validate PARSEC's design and mission architecture, we tested it in a flying arena, equipped with Optitrack motion capture cameras that sampled the aerial-base position and

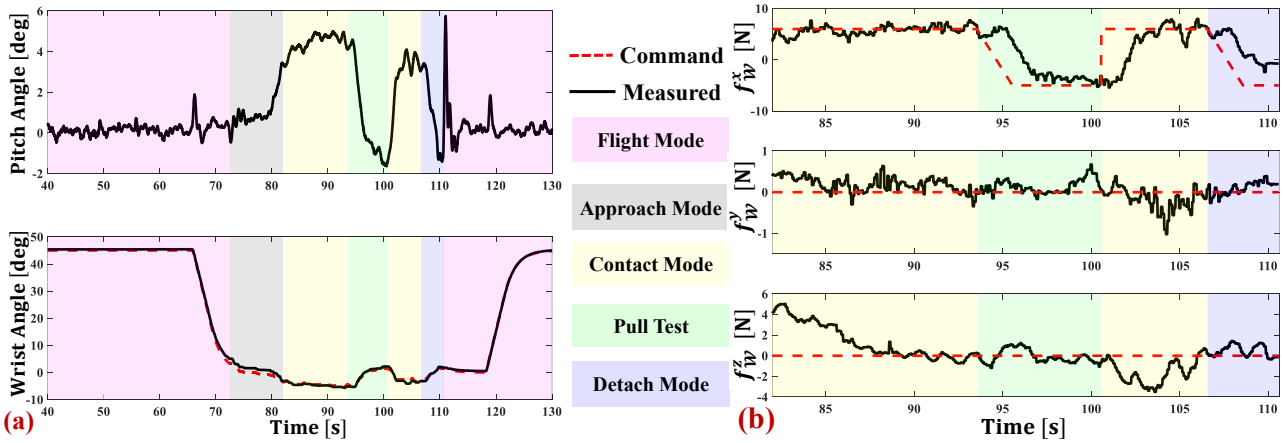

Fig. 7: Experiment Result: (a) Pitch and arm wrist angles versus time. (b) wall force setpoint and feedback during the deployment phase.

orientation at 200 Hz. This data served as the autopilot's position and attitude estimate. A Hex Cube Black flight controller runs a PX4 autopilot, which tracks desired attitude and thrust setpoints generated by the position and contact controllers running on an onboard computer (see Fig. 5).

Multirotor Subsystem

Component	Description	Mass (g)
Motors	T-Motor U3 700kV	128 (x6)
ESCs	Lunmenier 36A BLHeli_32	10 (x6)
Propellers	1355 Carbon Fiber Dual Blade	15 (x6)
Onboard Computer	Simply NUC Ruby R8	225
Flight Controller	Hex Pixhawk Cube 2.1	75
RC Receiver	Specktrum AR620	8
Batteries	6S Lipos, 1000 + 5200 mAh	170 + 760
Perception	Intel RealSense D435i	72

Manipulator Subsystem

Component	Description	Mass (g)
Linear Actuators	Actunoix T16-P 300mm	138(x2)
Wrist Servo	Robotis Dynamixel MX64T	126
Deployment Servo	Robotis Dynamixel AX12	55
Force Torque Sensor	ATI-IA Nano 25	61.4
Motor Controller 1	Roboclaw 2x7A	18
Motor Controller 2	Robotis U2D2	9

TABLE I: Key Off-the-shelf Components

We built a vertical wall with four 40cm $\times$ 40cm vesicular basalt rock tiles. They are analogous to Martian substrates. An anchoring location on the tiles is manually selected. We employ a tether as a safeguard. A $\sim$ 100 g passive weight eliminates tether slack and has minimal interference with the flight behavior due to an overall 5.4 kg system weight. The system's key off-the-shelf components are detailed in Table I while payload components are annotated in Fig. 4.

PARSEC successfully deployed and anchored a 430 g payload onto a vertical basalt surface (`https://youtu.be/fXwD3Tgk2cw`). Fig. 1 shows the system's behavior at four key stages. Fig. 7a plots the hexacopter pitch and wrist angles over the entire flight. During contact mode, a forward (positive) pitch can be seen in the upper plot as the vehicle orients its thrust towards the wall. The pull test and detach phases use a negative pitch angle. The wrist angle (lower plot) adapts to the vehicle pitch so as to keep a level payload. During the initial ($t = 69$ s) and final ($t = 120$ s) flight phases, the payload unfolds from and folds back to the stowed configuration. Fig. 7b shows the commanded and measured forces in the wall frame during wall contact. In the wall normal direction (plotted as the x-axis), we see a consistent 6 N pushing force during contact and a 5 N pull (negative) force during the pull test. In the detach mode, the force is never negative since the hexacopter has disengaged from the wall, which triggers a transition back to flight mode. In the vertical direction (z-axis) the 430 g payload weight is initially ($t = 82$ s) held by the arm. The payload weight is then gradually transferred to the wall, as the contact controller regulates zero vertical force.

VI. Conclusion and Future Work

We successfully demonstrated autonomous aerial deployment of a self-anchoring payload with substantial mass. This work serves as the proof-of-concept for mission concepts like the one depicted in Fig.2 and shows promise for future Mars science missions. PARSEC includes a 2 DoF counterbalancing manipulator to minimize CoG shifts and a deployable payload whose active microspines can anchor to steep natural surfaces. A four-state control architecture controlled contact forces while maintaining stable flight. Firmness of the anchor was detected via system sensors and verified through a pull test to ensure that the payload is securely anchored to the target. Future works will make the system viable for operation on Mars, which includes reconfigurable packaging to fit the system into an aeroshell for delivery to Mars and optimized the system's lift and weight ratio for the Mars atmosphere and gravity conditions. The ability to deploy multiple and heterogeneous payloads is one other topic of interest. Additionally, ongoing research aims to detect target surfaces areas with suitable grasp features and extensive testing of PARSEC under disturbances.

Acknowledgements

The authors acknowledge the valuable assistance of Kyle Uckert, Spencer Backus, and Runing Guan. This project is funded through JPL's President's and Director's Research and Development Fund. The work of M. Li is supported by a NASA Space Technology Research Fellowship (grant 80NSSC20K1166). Any opinions, findings, conclusions, or recommendations expressed in this paper do not necessarily reflect the views of the funding agencies.

REFERENCES

[1] J. Balaram, M. Aung, and M. Golombek, "The Ingenuity Helicopter on the Perseverance Rover," *Space Science Reviews*, vol. 217, 06 2021.

[2] W. Johnson, S. Withrow-Maser, L. Young, C. Malpica, W. J. Koning, W. Kuang, M. Fehler, A. Tuano, A. Chan, A. Datta *et al.*, "Mars science helicopter conceptual design," Tech. Rep., 2020.

[3] R. Lorenz, E. Turtle, J. Barnes, M. Trainer, D. Adams, K. Hibbard, C. Sheldon, K. Zacny, P. Peplowski, D. Lawrence, M. Ravine, T. McGee, K. Sotzen, S. MacKenzie, J. Langelaan, S. Schmitz, L. Wolfarth, and P. Bedini, "Dragonfly: A rotorcraft lander concept for scientific exploration at Titan," *Johns Hopkins APL Technical Digest (Applied Physics Laboratory)*, vol. 34, no. 3, pp. 374–387, Oct. 2018, publisher Copyright: © John Hopkins University. All rights reserved.

[4] K. Uckert, A. Parness, N. Chanover, E. J. Eshelman, N. Abcouwer, J. Nash, R. Detry, C. Fuller, D. Voelz, R. Hull, and et al., "Investigating habitability with an integrated rock-climbing robot and Astrobiology Instrument Suite," *Astrobiology*, vol. 20, no. 12, p. 1427–1449, 2020.

[5] S. Backus, J. Izraelevitz, J. Quan, R. Jitosho, E. Slavick, and A. Kalantari, "Design and Testing of an Ultra-Light Weight Perching System for Sloped or Vertical Rough Surfaces on Mars," 03 2020, pp. 1–12.

[6] A. Kalantari, K. Mahajan, D. Ruffatto, and M. Spenko, "Autonomous perching and take-off on vertical walls for a quadrotor micro air vehicle," in *2015 IEEE International Conference on Robotics and Automation (ICRA)*, 2015, pp. 4669–4674.

[7] W. R. T. Roderick, M. R. Cutkosky, and D. Lentink, "Bird-inspired dynamic grasping and perching in arboreal environments," *Science Robotics*, vol. 6, no. 61, 2021. [Online]. Available: https://www.science.org/doi/abs/10.1126/scirobotics.abj7562

[8] S. Kirchgeorg and S. Mintchev, "Hedgehog: Drone Perching on Tree Branches With High-Friction Origami Spines," *IEEE Robotics and Automation Letters*, vol. 7, no. 1, pp. 602–609, 2022.

[9] C. Geckeler and S. Mintchev, "Bistable Helical Origami Gripper for Sensor Placement on Branches," *Advanced Intelligent Systems*, p. 2200087.

[10] S. Kim, S. Choi, and H. J. Kim, "Aerial manipulation using a quadrotor with a two DOF robotic arm," in *2013 IEEE/RSJ International Conference on Intelligent Robots and Systems*, 2013, pp. 4990–4995.

[11] Y. Ohnishi, T. Takaki, T. Aoyama, and I. Ishii, "Development of a 4-joint 3-DOF robotic arm with anti-reaction force mechanism for a multicopter," in *2017 IEEE/RSJ International Conference on Intelligent Robots and Systems (IROS)*, 2017, pp. 985–991.

[12] A. Suarez, M. Perez, G. Heredia, and A. Ollero, "Cartesian Aerial Manipulator with Compliant Arm," *Applied Sciences*, vol. 11, p. 1001, 01 2021.

[13] A. Suarez, A. E. Jimenez-Cano, V. M. Vega, G. Heredia, A. Rodriguez-Castaño, and A. Ollero, "Design of a lightweight dual arm system for aerial manipulation," *Mechatronics*, vol. 50, pp. 30–44, 2018. [Online]. Available: https://www.sciencedirect.com/science/article/pii/S0957415818300011

[14] N. Imanberdiyev, S. Sood, D. Kircali, and E. Kayacan, "Design, development and experimental validation of a lightweight dual-arm aerial manipulator with a COG balancing mechanism," *Mechatronics*, vol. 82, p. 102719, 2022. [Online]. Available: https://www.sciencedirect.com/science/article/pii/S0957415821001781

[15] S. Hamaza, I. Georgilas, G. Heredia, A. Ollero, and T. Richardson, "Design, modeling, and control of an aerial manipulator for placement and retrieval of sensors in the environment," *Journal of Field Robotics*, vol. 37, no. 7, pp. 1224–1245, 2020. [Online]. Available: https://onlinelibrary.wiley.com/doi/abs/10.1002/rob.21963

[16] X. Meng, Y. He, Q. Li, F. Gu, L. Yang, T. Yan, and J. Han, "Contact Force Control of an Aerial Manipulator in Pressing an Emergency Switch Process," in *2018 IEEE/RSJ International Conference on Intelligent Robots and Systems (IROS)*, 2018, pp. 2107–2113.

[17] X. Meng, Y. He, and J. Han, "Hybrid Force/Motion Control and Implementation of an Aerial Manipulator towards Sustained Contact Operations," in *2019 IEEE/RSJ International Conference on Intelligent Robots and Systems (IROS)*, 2019, pp. 3678–3683.

[18] S. Hamaza, I. Georgilas, and T. Richardson, "Towards an Adaptive-Compliance Aerial Manipulator for Contact-Based Interaction," in *2018 IEEE/RSJ International Conference on Intelligent Robots and Systems (IROS)*, 2018, pp. 1–9.

[19] L. Meier, D. Honegger, and M. Pollefeys, "Px4: A node-based multithreaded open source robotics framework for deeply embedded platforms," in *2015 IEEE International Conference on Robotics and Automation (ICRA)*, 2015, pp. 6235–6240.